Strong polarization enhancement in asymmetric three-component ferroelectric superlattices

Ho Nyung Lee, Hans M. Christen, Matthew F. Chisholm, Christopher M. Rouleau & Douglas H. Lowndes

Condensed Matter Sciences Division, Oak Ridge National Laboratory, Oak Ridge, Tennessee 37831, USA

Theoretical predictions—motivated by recent advances in epitaxial engineering—indicate a wealth of complex behaviour arising in superlattices of perovskite-type metal oxides. These include the enhancement of polarization by strain[1,2] and the possibility of asymmetric properties in three-component superlattices[3]. Here we fabricate superlattices consisting of barium titanate ($BaTiO_3$), strontium titanate ($SrTiO_3$) and calcium titanate ($CaTiO_3$) with atomic-scale control by high-pressure pulsed laser deposition on conducting, atomically flat strontium ruthenate ($SrRuO_3$) layers. The strain in $BaTiO_3$ layers is fully maintained as long as the $BaTiO_3$ thickness does not exceed the combined thicknesses of the $CaTiO_3$ and $SrTiO_3$ layers. By preserving full strain and combining heterointerfacial couplings, we find an overall 50% enhancement of the superlattice global polarization with respect to similarly grown pure $BaTiO_3$, despite the fact that half the layers in the superlattice are nominally non-ferroelectric. We further show that even superlattices containing only single-unit-cell layers of $BaTiO_3$ in a paraelectric matrix remain ferroelectric. Our data reveal that the specific interface structure and local asymmetries play an unexpected role in the polarization enhancement.

Oxide heterostructures with atomically abrupt interfaces, defined by atomically flat surface terraces and single-unit-cell steps, can now be grown on well-prepared single-stepped substrates[4–7]. This advance has encouraged theoretical investigations that have led to predictions of new artificial materials[1–3,8–10]. The atomic-scale control of the combining of dissimilar materials is expected to produce striking property enhancements as well as new combinations of desired properties. Here we discuss the experimental realization of one of these predictions, the strain enhancement of ferroelectric polarization. The challenge associated with fabricating such strained structures—the deliberate and controlled deposition of up to hundreds of individual layers—remains a formidable task, for which the principal technique used has been high-vacuum molecular beam epitaxy[5,11]. However, many insulators do not yield the correct oxide stoichiometry (or expected resulting physical properties) when grown by molecular beam epitaxy. Furthermore, a shortage of electrically conducting oxide substrates and our still-limited understanding of the stability and growth mechanisms of conducting-film electrodes have hindered the electrical characterization of oxide superlattices.

To address these challenges, we have recently shown that atomically flat, electrically conducting $SrRuO_3$ electrodes can be grown with a surface quality that mimics that of the substrate (Fig. 1a)[7]. Pulsed laser deposition (PLD) has long been regarded as an effective method for synthesizing various oxide heterostructures[12–15], but obtaining atomically sharp interfaces has been difficult in the comparatively high-pressure processes needed to maintain oxygen stoichiometry. Here we demonstrate the growth by a high-pressure PLD technique of hundreds of individual perovskite layers of $BaTiO_3$, $SrTiO_3$ and $CaTiO_3$. These superlattices were grown with layer-by-layer control, yielding as-grown samples with compositionally abrupt interfaces, atomically smooth surfaces, and excellent ferroelectric behaviour that indicated oxygen stoichiometry.

Furthermore, whereas several earlier studies have used two-component $BaTiO_3/SrTiO_3$ structures[16–19], we focus here on three-component superlattices (TCSs). This breaks the inversion symmetry[3,20] that persists with most two-component superlattices, and provides additional freedom in tuning the average lattice parameter by using materials with smaller ($CaTiO_3$) and larger ($BaTiO_3$) unit-cell volumes than that of the substrate.

The PLD growth temperature was ~700 °C, with a relatively high oxygen pressure of 10 mtorr to ensure adequate oxidation. Growth conditions were optimized to require about 200 laser pulses per unit cell; this comparatively low deposition rate[21] allows us to terminate each layer precisely and thus minimize compositional intermixing[22]. Here we denote unit cells of $CaTiO_3$, $SrTiO_3$ and $BaTiO_3$ as C, S and B, respectively, and define a repeated stacking of z unit cells of $CaTiO_3$ on y unit cells of $BaTiO_3$ on x unit cells of $SrTiO_3$ as $S_xB_yC_z$, that is, starting the labelling from the bottom layer. The TCS structures studied include $S_xB_xC_x$ ($x = 1$, 2, 5 and 10), $S_xB_yC_x$ ($x = 2$ and $y = 4$, 6, 8), $S_xB_yC_y$ ($x = 4$ and $y = 2$) and $S_xB_xC_y$ ($x = 2$ and $y = 4$).

Figure 1 illustrates the film quality that results from the optimization of the deposition parameters. Cross-sectional atomic-number (Z)-contrast scanning transmission electron microscopy (Z-STEM) shows the compositional abruptness between the $SrRuO_3$ bottom electrode and a subsequently deposited $BaTiO_3$ film (Fig. 1a). In this image, a SrO termination of $SrRuO_3$ can be observed (solid arrow), consistent with RHEED (reflection high-energy electron diffraction) investigations by others[23]. Figure 1b depicts an atomic force microscopy (AFM) image of a $SrRuO_3$ film on a $SrTiO_3$ substrate. The single terrace steps (~0.4 nm in height) observed on this $SrRuO_3$ surface are a direct replica of those observed on the $SrTiO_3$ substrates, and thus provide an ideal starting condition for the TCS growth. In fact, we usually observed pronounced oscillations of the RHEED specular spot to persist even when growing superlattices up to 1 μm in thickness (data not shown). As shown in Fig. 1c, an AFM image of the top surface of a 200-nm-thick superlattice ($S_2B_2C_2$) exhibits a surface quality almost identical to that of the substrate and the $SrRuO_3$ film, again with single-unit-cell steps (~0.4 nm). A cross-sectional Z-contrast image of the corresponding structure in Fig. 1d indeed demonstrates the compositional abruptness of the layers. X-ray scans reveal that the entire structure grows 'coherently', that is, with a single value of the in-plane lattice parameter throughout the entire thickness. The long-range periodicity of this layering is further confirmed by X-ray diffraction (XRD): Fig. 1e shows an XRD θ–2θ scan of a $(S_2B_6C_2)_{50}$ superlattice grown on $SrRuO_3$(10 nm)/$SrTiO_3$, which exhibits clear superlattice peaks associated with the periodicity of the structure. Most structures also show a good peak separation between the Cu $K\alpha_1$ and $K\alpha_2$ lines (see also the XRD reciprocal space maps below), corresponding to well-defined lattice planes with high crystallinity.

To correlate strain and ferroelectric properties, XRD reciprocal space mapping (RSM) is used to quantify the strain state. Figure 2a shows an area scan through the 114 $BaTiO_3$ peak in reciprocal space of a 200-nm-thick $BaTiO_3$ film on a $SrRuO_3$(4 nm)/$SrTiO_3$ substrate. Peaks with identical Q_x (in-plane reciprocal lattice unit ($1/d$)) values correspond to crystalline material with identical in-plane lattice parameter. Thus the data of Fig. 2a show that the in-plane lattice parameter of the $BaTiO_3$ single film is larger than that of the substrate by about 2.5%; that is, the interfacial strain resulting from the substrate is largely relaxed (relieved by the formation of defects).

In contrast, interleaving $BaTiO_3$ layers with $SrTiO_3$ and $CaTiO_3$ layers in a superlattice structure can result in a material in which the in-plane lattice parameter is identical to that of the substrate (and thus smaller than in bulk $BaTiO_3$). Figure 2b shows the RSM for a $S_1B_1C_1$ and a $S_2B_2C_2$ structure; perfect in-plane matching in $S_xB_xC_x$ structures was observed even at values of $x = 10$. Such structures are particularly interesting, as they allow us to experimentally test

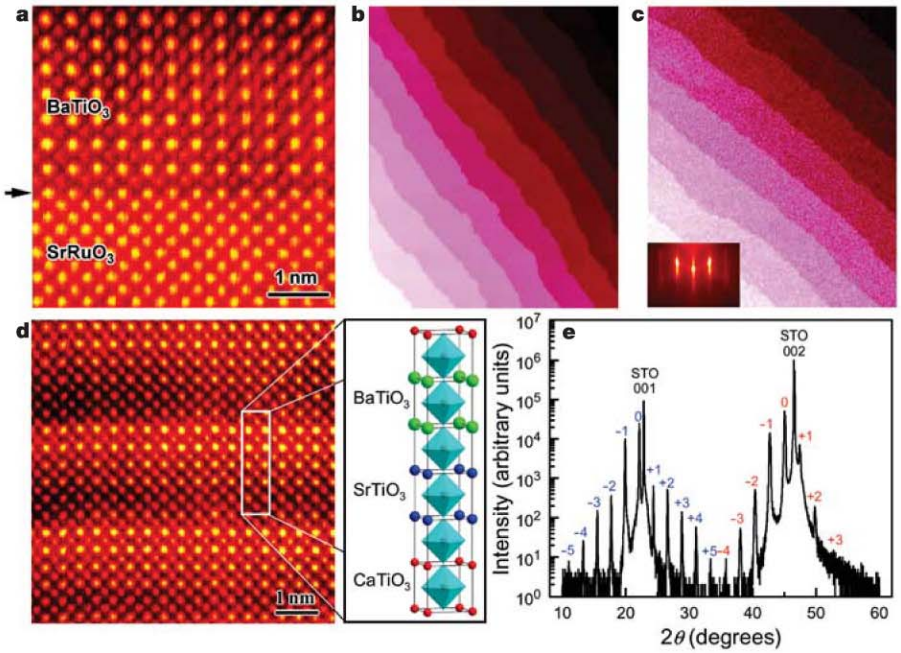

Figure 1 Atomic-scale flatness and compositional abruptness in surfaces and interfaces of conducting $SrRuO_3$ and artificial superlattices. **a**, Cross-sectional Z-contrast image of interface between $BaTiO_3$ and $SrRuO_3$ films, indicated by the black arrow. **b**,**c**, AFM topographic images (image size: $4 \times 5\ \mu m^2$) with single terrace steps (~0.4 nm) of $SrRuO_3$ (**b**) and of a 200-nm-thick $S_2B_2C_2$ superlattice (**c**). Inset in **c**, a RHEED pattern confirming the exceptionally smooth surface. **d**, Cross-sectional Z-contrast image of compositionally abrupt interfaces in $S_2B_2C_2$; the diagram shows its atomic structure. (The light-blue octahedra, and the red, green and blue spheres represent TiO_6, and Ca, Ba and Sr, respectively.) **e**, XRD θ–2θ scan of a $S_2B_6C_2$ superlattice, confirming the long-range periodicity and high crystallinity. The STO 001 and 002 peaks are from the $SrTiO_3$ substrate, and the first and second sets of superlattice peaks are marked with blue and red numbers, respectively.

results from calculations[1]. These calculations indicate a strain enhancement of the ferroelectric polarization in $BaTiO_3$ by about 50% as a consequence of an increase in the tetragonality (resulting from a decrease of the in-plane lattice parameter). Competing with this strain enhancement is the effect of the 'dilution' of the ferroelectric material in a paraelectric matrix. Density functional calculations on $SrTiO_3/BaTiO_3$ superlattices[1] indicate that the polarization is significantly larger than what would be expected from the $SrTiO_3$ and $BaTiO_3$ volume fractions alone, owing to electric-field-induced polarization in $SrTiO_3$. Calculations further predict ferroelectricity in superlattices containing only single-unit-cell layers of ferroelectric $BaTiO_3$ in an otherwise paraelectric matrix. In addition, even for structures containing single-unit-cell layers of $BaTiO_3$, the numerical results agree remarkably well with those from macroscopic considerations of independent ferroelectric and paraelectric slabs with dielectric constants ε_{FE} and ε_{PE}, respectively. In this electrostatic model, the average polarization is found to be

$$P_{avg} = P_{FE}[1 + (t_{PE}/t_{FE})(\varepsilon_{FE}/\varepsilon_{PE})]^{-1} \quad (1)$$

where P_{FE} is the polarization of the ferroelectric layer, and t_{FE} and t_{PE} are the thicknesses of ferroelectric and paraelectric layers, respectively.

For our TCSs containing one ferroelectric and two paraelectric components ($SrTiO_3$ with thickness t_{STO} and dielectric constant ε_{STO}, and $CaTiO_3$ with t_{CTO} and ε_{CTO}), the electrostatic considerations (equation (1)) are easily generalized by letting $t_{PE} = t_{STO} + t_{CTO}$ and $\varepsilon_{PE} = \varepsilon_{STO}\varepsilon_{CTO}(t_{STO} + t_{CTO})/(\varepsilon_{STO}t_{CTO} + \varepsilon_{CTO}t_{STO})$. Therefore, on the basis of electrostatics alone, the $S_1B_1C_1$ and $S_2B_2C_2$ structures should exhibit identical values of the polarization, whereas in fact the remanent polarization $P_r(S_1B_1C_1) \approx 3.0\,\mu C\,cm^{-2}$ and $P_r(S_2B_2C_2) \approx 5.4\,\mu C\,cm^{-2}$ (Fig. 2c), indicating that the interfaces have a significant effect. Moreover, as expected from previous work on $SrTiO_3/BaTiO_3$ superlattices[17,19], the dielectric constants (ε) as a function of electric field (E) as determined from the capacitance–voltage $C(V)$ curves at 100 kHz (Fig. 2d) are larger than that of the $BaTiO_3$ film.

Increasing the number of neighbouring Ba layers results in an increase of the enhancement of the polarization, pointing to the limitations of simple electrostatic considerations (equation (1)). The TiO_6 octahedra (which in the simplest picture are most responsible for the ferroelectric polarization) can be grouped into two classes (see below): those bound on both sides by the same A-site cations (for example, Ba-surrounded TiO_6) and those forming the interface between $BaTiO_3$, $SrTiO_3$ or $CaTiO_3$ (interfacial TiO_6).

To clarify the interplay between strain enhancement of the polarization and interfacial effects, we modified the number of interfaces and of neighbouring $BaTiO_3$ layers by interleaving identical $SrTiO_3$ and $CaTiO_3$ stackings with different numbers of $BaTiO_3$ layers (while keeping the total thickness fixed). Figure 3a–c shows RSMs (near the 114 $SrTiO_3$ reflection) of the $S_2B_4C_2$, $S_2B_6C_2$ and $S_2B_8C_2$ superlattices, respectively. A coherent in-plane lattice parameter is obtained only if the $BaTiO_3$ thickness in each superlattice period does not exceed the combined thickness of the $SrTiO_3$ and $CaTiO_3$ layers; consequently, a partial strain relaxation of 0.05% ($S_2B_6C_2$) and 1.21% ($S_2B_8C_2$) is observed in Fig. 3b and c, respectively. The evolution of the in-plane lattice parameter is shown in Fig. 4c as a function of the stacking sequence. In Fig. 4d, we show the polarization for the same structures. Clearly, the strongest polarization enhancement is achieved by the proper balancing of two competing requirements: the $BaTiO_3$ layers must be thick enough to contain a sufficient amount of non-interfacial TiO_6 octahedra (compare Fig. 4e), but thin enough to remain fully strained. This produces a maximum polarization for the $S_2B_4C_2$ structure (Fig. 4a). Despite the low volume fraction of 50%

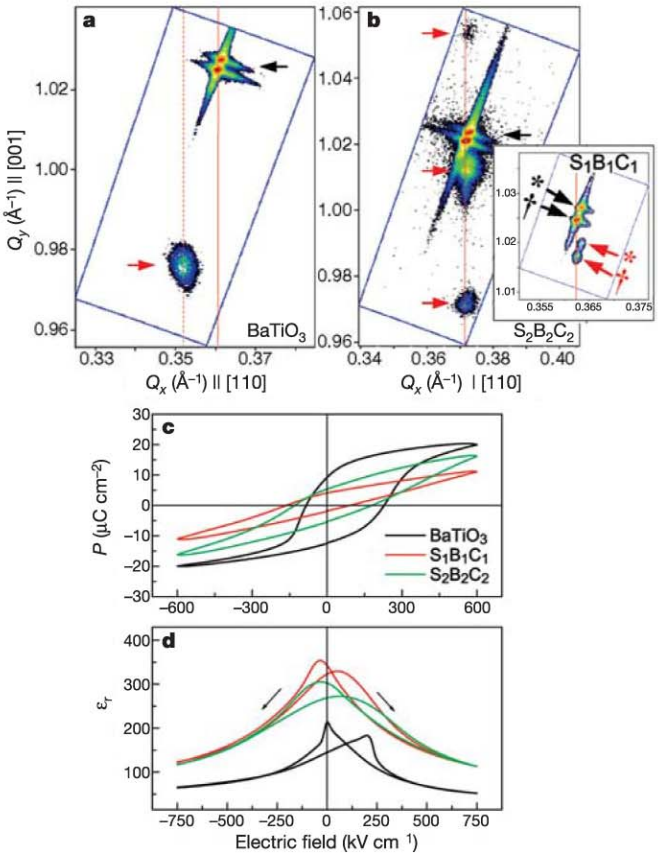

Figure 2 Strain states of a $BaTiO_3$ single film and superlattices on $SrRuO_3/SrTiO_3$ substrates and their ferroelectric properties. **a**, **b**, XRD-RSMs of a $BaTiO_3$ thin film and of a $S_2B_2C_2$ superlattice, respectively (Q_x and Q_y in units of $1/d$). A RSM of $S_1B_1C_1$ is also shown in the inset of **b** (same axes as main figure), showing clearly peaks from the Cu $K\alpha_1$ (†) and $K\alpha_2$ (*) lines. The solid red vertical lines mark the 114 $SrTiO_3$ Cu $K\alpha_1$ peak position, and the dotted red line that of $BaTiO_3$. Peaks marked with black and red arrows correspond respectively to reflections from the $SrTiO_3$ substrate, and from the film or superlattice layer and satellites. **c**, **d**, $P(E)$ at 100 Hz (**c**) and $\varepsilon(E)$ hysteresis loops at 100 kHz (**d**), from 200-nm-thick $BaTiO_3$ (black curves), $S_1B_1C_1$ (red) and $S_2B_2C_2$ (green).

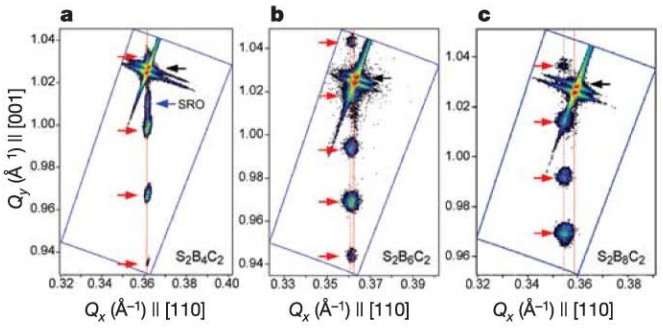

Figure 3 Evolution of the in-plane strain with changes in the thickness of $BaTiO_3$ layers for fixed thickness of $SrTiO_3$ and $CaTiO_3$. **a**–**c**, XRD-RSMs of $S_2B_4C_2$ (**a**), $S_2B_6C_2$ (**b**) and $S_2B_8C_2$ (**c**) superlattices, respectively, showing a gradual increase in the in-plane lattice parameter. (Solid and dotted red vertical lines mark the peak(s) of the substrate and superlattice, respectively.) The RSMs are recorded around the 114 $SrTiO_3$ reflection. Peaks marked with black and red arrows correspond respectively to reflections from the $SrTiO_3$ substrate, and those from the superlattice layer and satellites. The peak labelled "SRO" in **a** (indicated by the blue arrow) corresponds to the 114 reflection of the relatively thick $SrRuO_3$ film (16 nm).

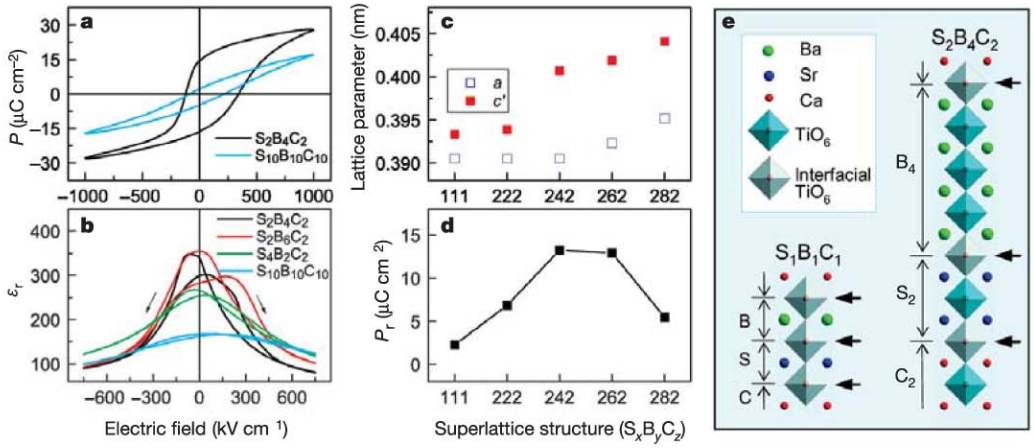

Figure 4 Polarization enhancement, changes in asymmetry, and evolution of strain in TCS structures. **a**, $P(E)$ curves of $S_2B_4C_2$ ($P_r \approx 16.5\,\mu C\,cm^{-2}$) and $S_{10}B_{10}C_{10}$ ($P_r \approx 3.5\,\mu C\,cm^{-2}$) at 1,000 kV cm^{-1}. (Note that this electric field is higher than that applied to measure the polarization of the $BaTiO_3$ film, whose polarization is near saturation at 400 kV cm^{-1}, whereas the $S_2B_4C_2$ requires a higher electric field (~700 kV cm^{-1})). **b**, $\varepsilon(E)$ curves of $S_2B_4C_2$ (black line), $S_2B_6C_2$ (red line), $S_4B_2C_2$ (green line) and $S_{10}B_{10}C_{10}$ (light blue line) showing differing degrees of asymmetry. **c**, In-plane (open squares) and out-of-plane (filled squares) lattice parameters of various superlattices. c' corresponds to the supercell c divided by the number of constituent perovskites in a supercell. **d**, P_r values from $E = \pm 750$ kV cm^{-1} loops. The partially relaxed $S_2B_8C_2$ structure was measured with $E = \pm 650$ kV cm^{-1} because of its lower breakdown strength. **e**, Diagrams of supercells showing the different local environments possible for the TiO_6-octahedra (bound by the same or different A-site cations). Heterointerfacial TiO_6 octahedra are shaded in grey and indicated by solid black arrows.

$BaTiO_3$, we observe an almost 50% increase in polarization ($P_r \approx 16.5\,\mu C\,cm^{-2}$ at 1 MV cm^{-1}) over that of the $BaTiO_3$ sample. This polarization is significantly larger than the value of $10.9\,\mu C\,cm^{-2}$ that would be predicted from electrostatic considerations alone, using bulk values for the effective dielectric constants $\varepsilon_{STO} = 300$, $\varepsilon_{CTO} = 186$ and $\varepsilon_{BTO} = 160$.

The fundamental difference between interfacial cells of $BaTiO_3$ and TiO_6-octahedra in an environment resembling that of bulk $BaTiO_3$ is further illustrated by considering structures of equal eight-unit-cell periodicity but different arrangements, that is, $S_4B_2C_2$, $S_2B_4C_2$ and $S_2B_2C_4$. All these structures are fully strained, and as pointed out above, the $S_2B_4C_2$ structure shows very strong polarization enhancement. In contrast, the other two samples of this series are characterized by $P_r < 3\,\mu C\,cm^{-2}$ (data not shown), slightly less than what would be expected from our $BaTiO_3$ data and the lower $BaTiO_3$ volume fraction (equation (1)).

The fact that equation (1) is insufficient to describe our data for three-component structures but almost perfectly reproduces the calculated behaviour of two-component $BaTiO_3/SrTiO_3$ super0 lattices points to additional effects that are operating here. One key weakness of applying equation (1) to the TCS configuration is the treatment of the $CaTiO_3/SrTiO_3$ bilayer as a simple dielectric with a passive interface. In reality, local distortions at the $SrTiO_3/CaTiO_3$ interface may also play a part, possibly even inducing a polarization in the neighbouring $SrTiO_3$ cells. Furthermore, for the samples considered here, the environment of the $BaTiO_3$ layers is strongly asymmetric. Considering the theoretically predicted enhancement of the polarization due to breaking of inversion symmetry will therefore be important in understanding these materials[3]. A previous report on similar TCS structures observed strong indications of asymmetry in $\varepsilon(E)$, but without ferroelectric hysteresis[11]. In contrast, the samples studied here exhibit strong ferroelectric switching with hysteresis curves both in $P(E)$ and $\varepsilon(E)$. However, asymmetry is observed here even in simple $BaTiO_3$ films. Therefore, we cannot neglect the possible effect of the dissimilar top and bottom electrodes (Pt and $SrRuO_3$, respectively) on the asymmetric behaviour. Nevertheless, close inspection of the $\varepsilon(E)$ curves in Fig. 4b shows a varying degree of asymmetry within each individual peak for different stacking sequences. This behaviour is not easily explained simply as a consequence of different electrode materials, but is expected to result from compositionally broken inversion symmetry[3].

This analysis of atomic-scale precision TCS structures thus leads to two observations. First, the use of three-component materials, as dictated by the need for near-perfect lattice matching to the substrate, reveals the subtle effects of a non-inversion-symmetric environment and the role of a large number of coupled heterointerfaces. Second, these structures have allowed the experimental verification of theoretical predictions of strain-enhanced ferroelectric polarization of $BaTiO_3$, even in structures containing a relatively small volume fraction of $BaTiO_3$. These results, together with the advance in pulsed laser deposition reported here, illustrate how enhancements of material properties—needed for applications in sensors, high-k dielectrics, and piezoelectric and ferroelectric devices—can be produced. □

Methods

Before growing the TCSs, epitaxial $SrRuO_3$ films (4–16 nm in thickness) were grown by PLD on single-stepped (001) $SrTiO_3$ substrates using a KrF excimer laser (wavelength $\lambda = 248$ nm) at 700 °C in 100 mtorr O_2. The TCSs were also grown by PLD at ~700 °C in 10 mtorr O_2 using sintered stoichiometric $CaTiO_3$ and $BaTiO_3$ targets, and a single-crystal $SrTiO_3$ target. We have previously shown that this combination of pressure and temperature lies within the stability range for our $SrRuO_3$ films[7]. In addition, the use of $CaTiO_3$ in the superlattice enhances the compressive strain, allows the average in-plane lattice parameter of the superlattice to match that of the substrate, and induces a wider range of elastic behaviour at the interface with $BaTiO_3$. The laser repetition rate and laser fluence were kept at 10 Hz and 2 J cm^{-2}, respectively. The deposition of each individual unit cell was monitored via the intensity oscillations of the specular spot in RHEED pattern. The topmost layer was capped by one or two unit cells of $SrTiO_3$ and the final thickness of all superlattices was fixed at 200 nm. For the electrical characterization, sputtered Pt top electrodes (100 μm in diameter) were used together with the conducting $SrRuO_3$ bottom electrode.

Received 17 September; accepted 3 December 2004; doi:10.1038/nature03261.

1. Neaton, J. B. & Rabe, K. M. Theory of polarization enhancement in epitaxial $BaTiO_3/SrTiO_3$ superlattices. *Appl. Phys. Lett.* **82,** 1586–1588 (2003).
2. Pertsev, N. A., Tagantsev, A. K. & Setter, N. Phase transitions and strain-induced ferroelectricity in $SrTiO_3$ epitaxial thin films. *Phys. Rev. B* **61,** R825–R829 (2000).
3. Sai, N., Meyer, B. & Vanderbilt, D. Compositional inversion symmetry breaking in ferroelectric perovskites. *Phys. Rev. Lett.* **84,** 5636–5639 (2000).
4. Kawasaki, M. *et al.* Atomic control of the $SrTiO_3$ crystal surface. *Science* **266,** 1540–1542 (1994).
5. Schlom, D. G. *et al.* Oxide nano-engineering using MBE. *Mater. Sci. Eng. B* **87,** 282–291 (2001).
6. Yamada, H. *et al.* Engineered interface of magnetic oxides. *Science* **305,** 646–648 (2004).
7. Lee, H. N., Christen, H. M., Chisholm, M. F., Rouleau, C. M. & Lowndes, D. H. Thermal stability of epitaxial $SrRuO_3$ films as a function of oxygen pressure. *Appl. Phys. Lett.* **84,** 4107–4109 (2004).

8. Okamoto, S. & Millis, A. J. Electronic reconstruction at an interface between a Mott insulator and a band insulator. *Nature* **428,** 630–633 (2004).
9. Junquera, J. & Ghosez, P. Critical thickness for ferroelectricity in perovskite ultrathin films. *Nature* **422,** 506–509 (2003).
10. Glinchuk, M. D. & Morozovska, A. N. The internal electric field originating from the mismatch effect and its influence on ferroelectric thin film properties. *J. Phys. Condens. Matter* **16,** 3517–3531 (2004).
11. Warusawithana, M. P., Colla, E. V., Eckstein, J. N. & Weissman, M. B. Artificial dielectric superlattices with broken inversion symmetry. *Phys. Rev. Lett.* **90,** 36802 (2003).
12. Lee, H. N., Hesse, D., Zakharov, N. & Gösele, U. Ferroelectric $Bi_{3.25}La_{0.75}Ti_3O_{12}$ films of uniform *a*-axis orientation on silicon substrates. *Science* **296,** 2006–2009 (2002).
13. Christen, H. M. *et al.* An improved continuous compositional-spread technique based on pulsed-laser deposition and applicable to large substrate areas. *Rev. Sci. Instrum.* **74,** 4058–4062 (2003).
14. Zheng, H. *et al.* Multiferroic $BaTiO_3$-$CoFe_2O_4$ nanostructures. *Science* **303,** 661–663 (2004).
15. Norton, D. P. Synthesis and properties of epitaxial electronic oxide thin-film materials. *Mater. Sci. Eng. R* **43,** 139–247 (2004).
16. Tabata, H., Tanaka, H. & Kawai, T. Formation of artificial $BaTiO_3$/$SrTiO_3$ superlattices using pulsed laser deposition and their dielectric properties. *Appl. Phys. Lett.* **65,** 1970–1972 (1994).
17. O'Neill, D., Bowman, R. M. & Gregg, J. M. Dielectric enhancement and Maxwell-Wagner effects in ferroelectric superlattice structures. *Appl. Phys. Lett.* **77,** 1520–1522 (2000).
18. Shimuta, T. *et al.* Enhancement of remanent polarization in epitaxial $BaTiO_3$/$SrTiO_3$ superlattices with asymmetric structure. *J. Appl. Phys.* **91,** 2290–2294 (2002).
19. Kim, J. *et al.* Large nonlinear dielectric properties of artificial $BaTiO_3$/$SrTiO_3$ superlattices. *Appl. Phys. Lett.* **80,** 3581–3583 (2002).
20. Ogawa, Y. *et al.* Nonlinear magneto-optical Kerr rotation of an oxide superlattice with artificially broken symmetry. *Phys. Rev. Lett.* **90,** 217403 (2003).
21. Muller, D. A., Nakagawa, N., Ohtomo, A., Grazul, J. L. & Hwang, H. Y. Atomic-scale imaging of nanoengineered oxygen vacancy profiles in $SrTiO_3$. *Nature* **430,** 657–661 (2004).
22. Lee, H. N. *et al.* Compositionally asymmetric tri-color superlattices grown by pulsed laser deposition. *Mater. Res. Soc. Symp. Proc.* **784,** C3.24 (2004).
23. Rijnders, G., Blank, D. H. A., Choi, J. & Eom, C. B. Enhanced surface diffusion through termination conversion during epitaxial $SrRuO_3$ growth. *Appl. Phys. Lett.* **84,** 505–507 (2004).

Acknowledgements This work was supported by the US Department of Energy under contract with the Oak Ridge National Laboratory, managed by UT-Battelle, LLC, as part of a BES NSET initiative on Nanoscale Cooperative Phenomena and of the LDRD programme.

Competing interests statement The authors declare that they have no competing financial interests.

Correspondence and requests for materials should be addressed to H.N.L. (hnlee@ornl.gov).